were violated by more than 0.3 Å and 5°, respectively. The total distance violation, and dihedral violation energies were 178.7 ± 2.4, 41.6 ± 0.9 and 0.50 ± 0.06 kcal mol^{-1}, respectively. The Lennard-Jones potential, which was not used during any refinement stage, was −526.2 ± 16.8 kcal mol^{-1} for the final structures. Ramachandran plot analysis of the final structures (residues 727–828) with Procheck-NMR[28] showed that 71.0 ± 0.6%, 23.8 ± 0.6%, 3.5 ± 0.2% and 1.7 ± 0.2% of the non-glycine and non-proline residues were in the most favourable, additionally allowed, generously allowed and disallowed regions, respectively. The corresponding values for the residues in the four α-helices (residues 727–743, 770–776, 785–802 and 807–827) were 88.9 ± 0.4%, 11.0 ± 0.4%, 0.1 ± 0.1% and 0.0 ± 0.0%, respectively. The structure of the bromodomain/acetyl-histamine complex was determined using the free-form structure and an additional 25 intermolecular and 5 intra-ligand NOE-derived distance restraints.

Site-direction mutagenesis. We prepared mutant proteins using the QuikChange site-directed mutagenesis kit (Stratagene). The presence of appropriate mutations was confirmed by DNA sequencing.

Ligand titration. We performed ligand titration by recording a series of 2D ^{15}N- and ^{13}C-HSQC spectra on the uniformly ^{15}N- and ^{15}N/^{13}C-labelled bromodomain (~0.3 mM), respectively, in the presence of different amounts of ligand concentration ranging from 0 to ~2.0 mM. The protein sample and the stock solutions of the ligands were all prepared in the same aqueous buffer containing 100 mM phosphate and 5 mM perdeuterated DTT at pH 6.5.

Received 12 January; accepted 8 April 1999.

1. Brownell, J. E. & Allis, C. D. Special HATs for special occasions: Linking histone acetylation to chromatin assembly and gene activation. *Curr. Opin. Genet. Dev.* **6,** 176–184 (1996).
2. Grunstein, M. Histone acetylation in chromatin structure and transcription. *Nature* **389,** 349–352 (1997).
3. Wolffe, A. P. Sinful repression. *Nature* **387,** 16–17 (1997).
4. Shikama, N., Lyon, J. & Thangue, N. B. L. The p300/CBP family: Integrating signals with transcription factors and chromatin. *Trends Cell Biol.* **7,** 230–236 (1997).
5. Haynes, S. R. *et al*. The bromodomain: A conserved sequence found in human, *Drosophila* and yeast proteins. *Nucleic Acids Res.* **20,** 2603–2603 (1992).
6. Jeanmougin, F., Wurtz, J. M., Douarin, B. L., Chambon, P. & Losson, R. The bromodomain revisited. *Trends Biochem. Sci.* **22,** 151–153 (1997).
7. Brownell, J. E. *et al*. *Tetrahymena* histone acetyltransferase A: A homolog to yeast Gcn5p linking histone acetylation to gene activation. *Cell* **84,** 843–851 (1996).
8. Ogryzko, V. V., Schiltz, O. L., Russanova, V., Howard, B. H. & Nakatani, Y. The transcriptional coactivators p300 and CBP are histone acetyltransferases. *Cell* **87,** 953–959 (1996).
9. Bannister, A. J. & Kouzarides, T. The CBP co-activator is a histone acetyltransferase. *Nature* **384,** 641–643 (1996).
10. Yang, X.-J., Ogryzko, V. V., Nishikawa, J.-I., Howard, B. H. & Nakatani, Y. A p300/CBP-associated factor that competes with the adenoviral oncoprotein E1A. *Nature* **382,** 319–324 (1996).
11. Puri, P. L. *et al*. Differential roles of p300 and PCAF acetyltransferases in muscle differentiation. *Cell* **1,** 35–45 (1997).
12. Richardson, J. S. The anatomy and taxonomy of protein structure. *Adv. Protein Chem.* **34,** 167–339 (1981).
13. Presnell, S. R. & Cohen, F. E. Topological distribution of four-α-helix bundles. *Proc. Natl Acad. Sci. USA* **86,** 6592–6596 (1989).
14. Weber, P. C. & Salemme, F. R. Structural and functional diversity in 4-α-helical proteins. *Nature* **287,** 82–84 (1980).
15. Kurokawa, R. *et al*. Differential use of CREB binding protein–coactivator complex. *Nature* **279,** 700–703 (1998).
16. Chen, H. *et al*. Nuclear receptor coactivator ACTR is a novel histone acetyltransferase and forms a multimeric activation complex with P/CAF and CBP/p300. *Cell* **90,** 569–580 (1997).
17. Kuo, M.-H. *et al*. Transcription-linked acetylation by Gcn5p of histone H3 and H4 at specific lysines. *Nature* **383,** 269–272 (1996).
18. Dutnall, R. N., Tafrov, S. T., Sternglanz, R. & Ramakrishnan, V. Structure of the histone acetyltransferase Hat1: A paradigam for the GCN5-related N-acetyltransferase superfamily. *Cell* **94,** 427–438 (1998).
19. Pawson, T. Protein modules and signalling networks. *Nature* **373,** 573–580 (1995).
20. Geogakopoulos, T., Gounalaki, N. & Thireos, G. Genetic evidence for the interaction of the yeast transcriptional co-activator proteins GCN5 and ADA2. *Mol. Gen. Genet.* **246,** 723–728 (1995).
21. Yamazaki, T., Lee, W., Arrowsmith, C. H., Mahandiram, D. R. & Kay, L. E. A suite of triple resonance NMR experiments for the backbone assignment of ^{15}N, ^{13}C, ^{2}H labeled proteins with high sensitivity. *J. Am. Chem. Soc.* **116,** 11655–11666 (1994).
22. Clore, G. M. & Gronenborn, A. M. Multidimensional heteronuclear nuclear magnetic resonance of proteins. *Meth. Enzymol.* **239,** 249–363 (1994).
23. Logan, T. M., Olejniczak, E. T., Xu, R. X. & Fesik, S. W. A general method for assigning NMR spectra of denaturated proteins using 3D HC(CO)NH-TOCSY triple resonance experiments. *J. Biomol. NMR* **3,** 225–231 (1993).
24. Neri, D., Szyperski, T., Otting, G., Senn, H. & Wüthrich, K. Stereospecific nuclear magnetic resonance assignments of the methyl groups of valine and leucine in the DNA-binding domain of the 434 repressor by biosynthetically directed fractional ^{13}C labeling. *Biochemistry* **28,** 7510–7516 (1989).
25. Johnson, B. A. & Blevins, R. A. NMRView: A computer program for the visualization and analysis of NMR data. *J. Biomol. NMR* **4,** 603–614 (1994).
26. Brünger, A. T. *X-PLOR Version 3.1: A System for X-Ray Crystallography and NMR* (Yale University Press, New Haven, 1993).
27. Nilges, M. & O'Donoghue, S. Ambiguous NOEs and automated NOE assignment. *Progr. NMR Spectr.* **32,** 107–139 (1998).
28. Laskowski, R. A., Rullmannn, J. A., MacArthur, M. W., Kaptein, R. & Thornton, J. M. AQUA and PROCHECK-NMR: Programs for checking the quality of protein structures solved by NMR. *J. Biomol. NMR* **8,** 477–486 (1996).
29. Carson, M. Ribbons 2.0. *J. Appl. Crystallogr.* **24,** 958–961 (1991).
30. Nicholls, A., Bharadwj, R. & Honig, B. GRASP: Graphical representation and analysis of surface properties. *Biophys. J.* **64,** 166–170 (1993).

Acknowledgements. We thank M. Sattler, M. Nilges, M. Rosen, R. P. Meadows, and C. Escalante for technical advice; O. Plotnikova for assistance in the preparation of mutant proteins; I. Wolf for peptide synthesis; and D. Logothetis, H. Weinstein, L. Shapiro, R. Margolskee and A. Farooq for their suggestions and for critical reading of the manuscript. This work was supported by discretionary funds from the Mount Sinai School of Medicine (to M.M.Z.) and NIH grants (to A.A.).

Correspondence and requests for materials should be addressed to M.M.Z. (e-mail: zhoum@inka.mssm.edu). Coordinates for the NMR structure of the P/CAF bromodomain have been deposited in the Brookhaven Protein Data Bank under accession code 1B91.

Enzyme dynamics and hydrogen tunnelling in a thermophilic alcohol dehydrogenase

Amnon Kohen*, Raffaele Cannio†, Simonetta Bartolucci‡ & Judith P. Klinman*§

** Department of Chemistry and § Department of Molecular and Cell Biology, University of California at Berkeley, Berkeley, California 94720, USA*
† ISA CNR, via Roma, 83100 Avellino, Italy
‡ Dipartimento di Chimica Organica e Biologica, Università di Napoli "Rederico II", via Mezzocannone 16, 80134 Napoli, Italy

Biological catalysts (enzymes) speed up reactions by many orders of magnitude using fundamental physical processes to increase chemical reactivity. Hydrogen tunnelling has increasingly been found to contribute to enzyme reactions at room temperature[1]. Tunnelling is the phenomenon by which a particle transfers through a reaction barrier as a result of its wave-like property[1–3]. In reactions involving small molecules, the relative importance of tunnelling increases as the temperature is reduced[4]. We have now investigated whether hydrogen tunnelling occurs at elevated temperatures in a biological system that functions physiologically under such conditions. Using a thermophilic alcohol dehydrogenase (ADH), we find that hydrogen tunnelling makes a significant contribution at 65 °C; this is analogous to previous findings with mesophilic ADH at 25 °C (ref. 5). Contrary to predictions for tunnelling through a rigid barrier, the tunnelling with the thermophilic ADH decreases at and below room temperature. These findings provide experimental evidence for a role of thermally excited enzyme fluctuations in modulating enzyme-catalysed bond cleavage.

Structural studies of enzymes have influenced our view of catalysis enormously by providing three-dimensional pictures of active sites. But although these time-averaged structures are extremely useful as a starting point for evaluating and modelling catalysis, they generally fail to incorporate the wide range of dynamic motion that can occur in proteins[6]. It is a major experimental challenge to examine the relationship between the dynamics of a protein and its activity. Various studies have shown a relationship between protein dynamics and the physical steps of the enzymatic process, that is, those steps involving the formation and breakdown of catalytic complexes[7,8], but a far greater problem is whether protein dynamics have a direct role in the catalysis of bond forming and cleaving. Our present findings on hydrogen transfer under physiological conditions cannot be explained without invoking both quantum mechanics and enzyme dynamics.

Recent literature has demonstrated the importance of quantum-mechanical tunnelling in enzyme-catalysed hydrogen-transfer reactions[1]. Indirect evidence that dynamical motion is involved comes from the demonstration that surface glycosylation of glucose oxidase decreases the extent of quantum behaviour observed in

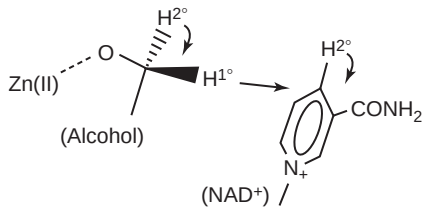

Figure 1 Motion of the primary (1°) and secondary (2°) hydrogens in the reaction of alcohol dehydrogenase.

enzyme-catalysed hydrogen transfer[9]. The present study investigated hydrogen tunnelling in an alcohol dehydrogenase from *Bacillus stearothermophilus* LLD-R strain, a thermophilic protein (referred to as ADH-hT) that normally functions at 65 °C (refs 10,11). ADH-hT is very similar to the more extensively studied mesophilic ADHs (from horst liver and yeast), having 55% sequence identity, including conservation of most active-site residues, and containing the structural and catalytic zinc ions found in mesophilic ADHs. With thermophilic enzymes, the study of catalysis as a function of temperature has often demonstrated biphasic Arrhenius behaviour, with an increased enthalpy of activation at temperatures below the break-point in plots of ln (*k*) against the reciprocal of the absolute temperature (1/*T*) (refs 12–15). This behaviour has been attributed to increased protein rigidity at reduced temperatures.

Our study of hydrogen tunnelling as a function of temperature using thermophilic ADH-hT allows us to examine how protein mobility affects the contribution of hydrogen tunnelling to the reaction rate. Specifically, if protein mobility is a prerequisite for effective tunnelling, a decreased tunnelling contribution is predicted as the temperature is reduced below the optimal temperature for ADH-hT. This is in direct contrast to models of hydrogen tunnelling through a rigid barrier, which predict an increased contribution of tunnelling to rate with decreased temperature[3,4].

We measured tunnelling with ADH-hT according to protocols previously established for demonstrating tunnelling with mesophilic enzymes[1,5]. One of these protocols involves the competitive measurement of multiple kinetic isotope effects (KIEs, that is, k_D/k_T and k_H/k_T, where k_H, k_D and k_T are rate constants for reaction of protium, deuterium and tritium. It is expected that $(k_D/k_T)^{3.3} = k_H/k_T$ under conditions of semi-classical behaviour[16], that is, when tunnelling makes no contribution to reaction rate. Measurements conducted under conditions where the hydrogen-transfer step is only partially rate limiting deflate the exponent to below 3.3, while enhanced tunnelling of protium in relation to deuterium can lead to an exponent larger than 3.3 (refs 16–18). Isotope effects can be measured in either the primary (1°) or the secondary (2°) position (see Fig. 1). Exponents larger than 3.3 are most readily detected in secondary KIE measurements under conditions of both tunnelling and coupled motion between the primary and secondary hydrogens of the substrate[16–18] (Fig. 1).

Figure 2a–d shows the temperature dependencies measured for the primary and secondary k_H/k_T and k_D/k_T isotope effects with ADH-hT, and indicates that the KIEs are essentially temperature independent between 65 °C and 30 °C but rise steeply with temperature below 30 °C. The exponents relating H/*T* and D/*T* ($(k_D/k_T)^{exponent} = k_H/k_T$) for secondary KIEs (Fig. 2f) are much higher than the semi-classical limit between 65 °C to 30 °C and decrease towards semi-classical values as the temperature is reduced from 30 °C to 5 °C. The data in Fig. 2 provide clear evidence for significant hydrogen tunnelling at elevated temperature with ADH-hT (at its physiological temperature). The decrease in the secondary exponents at temperatures below 30 °C cannot be due to a change in the rate-determining step that makes the hydrogen-transfer step less rate determining, because primary exponents are not suppressed

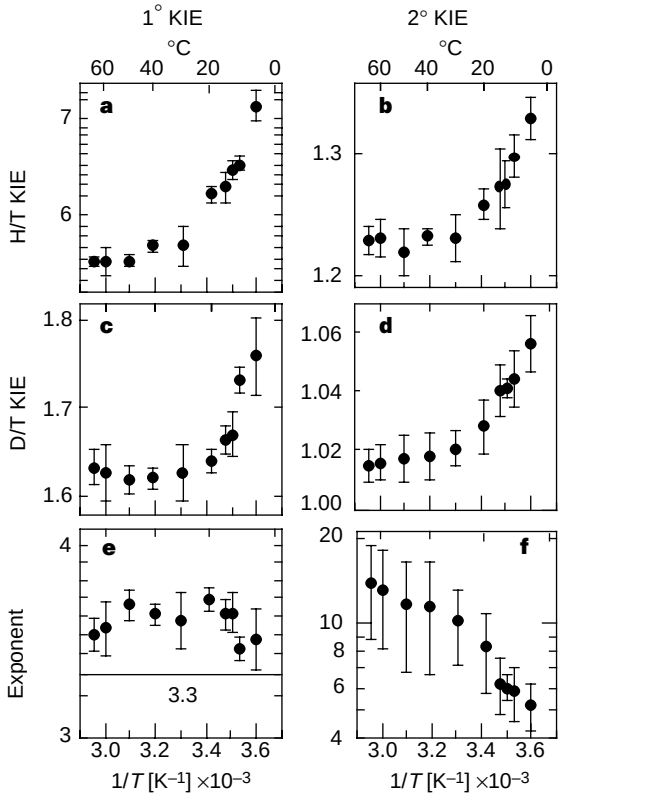

Figure 2 Competitive primary (1°) and secondary (2°) kinetic isotope effects (KIEs) on logarithmic abscissa versus 1/*T*, ranging from 5 °C to 65 °C. **a**, 1° H/T KIEs and **b**, 2° H/T KIEs were measured simultaneously for the ADH-hT-catalysed oxidation of benzyl alcohol by NAD^+. **c**, 1° D/T KIEs and **d**, 2° D/T KIEs were measured likewise. **e**, **f**, The exponent that relates 1° and 2° H/T and D/T measurements. The solid line in **e** indicates the semi-classical upper limit of 3.3. The relationship of H/T to D/T KIE is calculated from: $k_H/k_T = (k_D/k_T)^{exponent}$. Standard errors (error bars) are calculated from:

$$\Delta\text{exponent} = \sqrt{\left(\frac{\Delta(k_H/k_T)}{k_H/k_T}/\ln(k_D/k_T)\right)^2 + \left(\frac{\Delta(k_D/k_T)}{k_D/k_T}\frac{\ln(k_H/k_T)}{(\ln(k_D/k_T))^2}\right)^2}$$

below 3.3 (Fig. 2e), and the measured primary KIEs become larger as the temperature is reduced below 30 °C (Fig. 2a, c). Because rigid models predict that tunnelling will be more significant at reduced temperatures, Fig. 2 indicates a temperature-dependent transition in the protein's behaviour that impairs hydrogen tunnelling.

A second major tool for investigating hydrogen tunnelling comes from comparing Arrhenius plots for the reaction of the isotopes of hydrogen (Fig. 3). It is well accepted that for reactions with no tunnelling contribution, the intercept (*A*) of Arrhenius plots for L/*T* KIEs, denoted as A_L/A_T (where L is H or D)) will be close to unity (for example, Fig. 3, region I)[2]. By contrast, when protium tunnelling is greater than with deuterium or tritium, the experimentally measured KIEs will result in inverse values for A_L/A_T (for example, Fig. 3, region II)[2]. Conversely, when tunnelling through a rigid barrier dominates a reaction, slopes of Arrhenius plots for all isotopes approach zero and their A_L/A_T values are significantly greater than unity (Fig. 3, region III)[4]. Analysis of the primary KIE data in Fig. 2 allows an estimate of both A_H/A_T and A_D/A_T (see Table 1). Once again, these data implicate more tunnelling at the higher temperature range (65 °C to 30 °C, $A_L/A_T > 1$) than between 30 °C and 5 °C ($A_L/A_T < 1$).

Our finding of values for $A_L/A_T > 1$ between 65 °C and 30 °C is particularly intriguing in the context of the mechanism by which ADH-hT facilitates tunnelling. If the behaviour of ADH-hT is analogous to regime III of Fig. 3 (tunnelling through a rigid barrier),

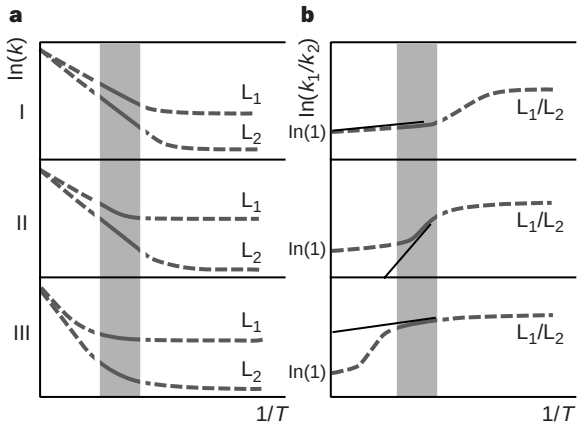

Figure 3 a, Arrhenius plot of ln (*k*) against 1/*T* for a light isotope (L_1) and a heavier isotope (L_2). **b**, Arrhenius plot of ln (k_1/k_2) against 1/*T*. The experimental temperature range is highlighted in grey. The L_1/L_2 KIE on the Arrhenius pre-exponential factors (A_1/A_2) is the intercept of the tangent to the curve at the experimental temperature range (dark lines). Three experimental systems are presented: system I, with no tunnelling contribution, A_1/A_2 of unity; system II, with some tunnelling contribution to the L_1 reaction whose plot curves upward, $A_1/A_2 < 1$; system III, where both isotopes tunnel significantly, $A_1/A_2 > 1$. (Reproduced with some modification from ref. 1.)

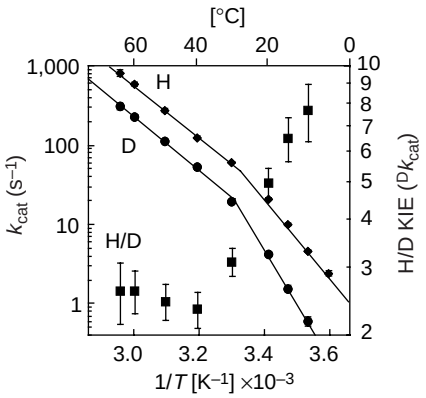

Figure 4 Arrhenius plots of k_{cat} for protonated (diamonds) and deuterated (circles) substrates (left abscissa), and Arrhenius plot of their KIE (squares) (right abscissa).

the experimental enthalpy of activation ($\Delta H^{\ddagger}$) for C–L-bond cleavage would be expected to be close to zero and KIEs would be enormous[4]. In contrast, if tunnelling occurs by a vibrationally enhanced mechanism, values measured for the individual $\Delta H^{\ddagger}$ may be large and the magnitude of isotope effects could fall in the semi-classical range[19]. To investigate this distinction, we analysed non-competitive isotope effects by comparing the rate of oxidation of [1 − $^1H_2$]-alcohol by ADH-hT with that of [1 − $^2H_2$]-alcohol.

We measured initial velocities while varying both alcohol and nicotinamide adenine dinucleotide (NAD^+) concentrations, thus allowing the rate constant when both substrates are at saturating concentrations (k_{cat}), to be estimated as a function of temperature. The resulting Arrhenius plots (Fig. 4) have slopes at elevated temperatures that are both large and essentially identical for protonated and deuterated substrates, with $A_H/A_D > 1$ (Table 2). Below the transition temperature of about 30 °C, the slopes for protonated and deuterated substrates begin to diverge, with increased $\Delta H^{\ddagger}$ values and $A_H/A_D < 1$. These non-competitive rate data lead to several key confirmatory findings. First, the fact that the curves for protonated and deuterated substrates break at similar temperatures argues against a change in the rate-determining step, once again implicating a physical change in the protein as the origin of the observed behaviour. This is supported by the finding that the size of the KIE increases below 30 °C. Additionally, the non-competitive KIEs on k_{cat} and k_{cat}/K_m are similar (data not shown), consistent with a random equilibrium kinetic mechanism in which C–H-bond cleavage is close to fully rate-determining across the full temperature range. As was concluded from the competitive KIEs described above, the different $\Delta H^{\ddagger}$ values for protonated alcohol and deuterated alcohol below 30 °C indicate greater semi-classical behaviour, that is, a reduction in tunnelling as the temperature is lowered.

Our results show that tunnelling is very significant at elevated temperatures under conditions where the thermophilic enzyme is optimally functional. The extent of tunnelling decreases with temperature, opposite to the trend predicted from simple chemical models and measurements, and indicating a transition for the protein at approximately 30 °C. In light of the substantial evidence for an increased rigidity of thermophilic enzymes with reduced temperature[12,13,15,20], we ascribe the decrease in tunnelling at reduced temperatures to reduced protein mobility required to facilitate tunnelling. This model of vibrationally enhanced tunnelling is consistent with the high-temperature data in which $\Delta\Delta H^{\ddagger}$ for protonated compared with deuterated substrate is close to zero while the individual values for $\Delta H^{\ddagger}$ remain sizeable. Although it has been postulated theoretically that enzymes work by dynamically enhanced mechanisms (see below), the present results provide the first experimental evidence to support this.

Since the work of Vol'kenshtein[21], increasingly sophisticated theories have been advanced describing a possible link between protein motion and hydrogen tunnelling[22–26]. Work by Borgis and Hynes[25], Bruno and Bialek[26,27,29] and most recently Antoniou and Schwartz[23–27] have stressed the importance of orthogonal coordinates involving a temperature-dependent, isotope-independent variation in the relative energy levels for reactant and product, and a temperature and isotope-dependent variation of the internuclear distance. A key feature of all these models is that the temperature dependence for the tunnelling reaction derives from the reaction exothermicity and the energetic terms for protein rearrangements, that is, $\Delta H^{\ddagger}$ need not reflect the barrier height for C–H-cleavage as formulated according to classical transition-state theory[3]. Although a change in the average protein conformation cannot be ruled out, the activity transition for ADH-hT can be understood in the context of a motion(s) that decreases below 30 °C. At reduced temperatures the amplitude of the promoting vibration(s) for ADH-hT decreases below a level required for effective tunnelling. The reaction begins to approximate more classical behaviour with less tunnelling, an increased enthalpy of activation and a rate that is an order of magnitude less than that predicted from the high-temperature behaviour.

Table 1 A_L/A_T from primary KIEs measured under competitive conditions

Temperature range	A_H/A_T	A_D/A_T
5–30 °C	0.26 (±0.23)	0.23 (±0.14)
Semi-classical*	0.60 to 1.67	0.90 to 1.22
30–65 °C	4.3 (±0.6)	1.73 (±0.26)

A_L/A_T are isotope effects on Arrhenius pre-exponential factors where L is H or D (see text and Fig. 2).
* Refs 2, 19.

Table 2 Parameters derived from non-competitive measurements

	Temperature range (°C)	
Parameter	5–30	30–65
$\Delta H^{\ddagger}_{30\,°C}$ (H) (kcal mol^{-1})	23.6 (±0.6)	14.6 (±0.3)
$\Delta H^{\ddagger}_{30\,°C}$ (D) (kcal mol^{-1})	31.4 (±1.7)	15.1 (±0.5)
$\Delta H^{\ddagger}$(D) − $\Delta H^{\ddagger}$(H) (kcal mol^{-1})	7.8 (±1.8)	0.5 (±0.6)
A_H/A_D	1×10^{-5} ($\pm 1 \times 10^{-5}$)	2.2 (±1.1)

See also Fig. 4.

Our findings have important implications for the catalytic behaviour of enzymes. The comparison of thermophilic and mesophilic species (25 °C for the yeast ADH, 65 °C for ADH-hT) verifies the old notion that different enzymes impose similar environments on their active sites at their physiological temperatures[13,28]. Our comparison of the tunnelling behaviour for the thermophilic enzyme across a sizeable temperature range (65–5 °C) suggests a role for protein mobility in C–H-bond cleavage. It is perhaps not surprising that, for C–H-bond cleavage reactions, a partitioning of thermal energy into low-frequency protein modes is a major factor. These modes can become significantly excited at ambient temperature, in contrast to the C–H stretching mode, which is expected to be largely confined to its zero-point energy level. The implication of protein dynamics in modulating chemical steps makes it easier to understand why biomimetic models, as well as catalytic antibodies, often fall short of the rate accelerations observed with enzymes. The idea of a dynamic coupling of protein vibrational modes into the chemical reaction coordinate should increasingly aid our understanding of biological catalysis.

Note added in proof: Studies by Basram *et al.* (*Biochemistry* **38,** 3218–3222 (1999)) on the hydrogen transfer catalysed by a mesophilic methylamine dehydrogenase show isotope effects and enthalpies of activation consistent with a role for vibrationally enhanced tunnelling. □

Methods

Enzyme preparation. ADH-hT from *B. stearothermophilus* LLD-R strain was expressed and purified as described before[10,11] with minor modification.

Competitive KIEs. All competitive KIEs reported were measured under Ar with 4 mM NAD^+, 50 mM potassium phosphate, pH 7.0, 300 mM semicarbazide hydrochloride, and 1.5 mM dithiothreitol, between 5 and 65 °C. The temperature was thermostated to ±0.1 °C in a Neslab water bath, and the pH was adjusted at the experimental temperature. The kinetic experiments were conducted and analysed as described previously[5], with minor modifications. Each reported KIE is an average of 14–35 points measured in several different experiments.

Non-competitive measurements. Initial velocities were measured over a temperature range of 5–65 °C in 50 mM potassium phosphate, pH 7.0, by following the 340-nm absorption of the product NADH using $[1,1-{}^1H_2]$ or $[1,1-{}^2H_2]$ benzyl alcohol. NAD^+ concentrations were in the range 0.2–4.0 mM and alcohol concentrations were 0.75–20 mM. Cofactor concentration above 10 mM and alcohol concentration above 50 mM showed some substrate inhibition. For each k_{cat} measurement, five substrate concentrations were varied with five cofactor concentrations and the initial velocities were fitted to the equation: $v = k_{cat}[E][A][B]/(Kia[B] + K_A[B] + K_B[A] + [A][B])$, where [E] is the enzyme concentration, [A] and [B] are the cofactor and substrate concentrations, respectively, K_A and K_B are their Michaelis constants and *Kia* is the cofactor dissociation constant. The slope and intercept of the Arrhenius plots at the different temperature ranges were obtained from the error-weighted nonlinear fit. The ratio of the values of the protonated versus the deuterated substrates yielded the H/D KIEs.

Received 26 October 1998; accepted 16 March 1999.

1. Kohen, A. & Klinman, P. J. Enzyme catalysis: beyond classical paradigms. *Acc. Chem. Res.* **31,** 397–404 (1998).
2. Bell, R. P. *The Tunneling Effect in Chemistry* (Chapman & Hall, London, 1980).
3. Steinfeld, J. I., Francisco, J. S. & Hase, W. L. (eds) *Chemical Kinetics and Dynamics* (Prentice Hall, Upper Saddle River, NJ, 1998).
4. Benderskii, V. A., Makarov, D. E. & Wight, C. A. *Adv. Chem. Phys.* **88,** 151–207 (1994).
5. Cha, Y., Murray, C. J. & Klinman, J. P. Hydrogen tunneling in enzyme reactions. *Science* **243,** 1325–1330 (1989).
6. Brooks, C. L. I., Karplus, M. & Pettitt, B. M. *Adv. Chem. Phys.* **71,** 14–23; 33–59; 75–233; (1988).
7. Rasmussen, B. F., Stock, A. M., Ringe, D. & Petsko, G. A. Crystalline ribonuclease-A loses function below the dynamical transition at 220-K. *Nature* **357,** 423–424 (1992).
8. Rudd, P. M. *et al.* Glycoforms modify the dynamic stability and functional activity of an enzyme. *Biochemistry* **33,** 17–22 (1994).
9. Kohen, A., Jonsson, T. & Klinman, P. J. Effect of protein glycosylation on catalysis: changes in hydrogen tunneling and enthalpy of activation in the glucose oxidase reaction. *Biochemistry* **36,** 2603–2611 (1997).
10. Cannio, R., Rossi, M. & Bartolucci, S. A few amino acid substitutions are responsible for the higher thermostability of a novel NAD(+)-dependent bacillar alcohol dehydrogenase. *Eur. J. Biochem.* **22,** 345–352 (1994).
11. Guagliardi, A. *et al.* Purification and characterization of the alcohol dehydrogenase from a novel strain of *bacillus stearothermophilus* growing at 70 °C. *Int. J. Biochem. Cell Biol.* **28,** 239–246 (1996).
12. Lakatos, S., Halasz, G. & Zavodszky, P. Conformational stability of lactate dehydrogenase from *Bacillus thermus-aquaticus*. *Biochem. Soc. Trans.* **6,** 1195–1197 (1978).
13. Zavodszky, P., Kardos, J., Svingor, A. & Petsko, G. A. Adjustment of conformational flexibility is a key event in the thermal adaptation of protein. *Proc. Natl Acad. Sci. USA* **95,** 7406–7411 (1998).
14. Varley, P. G. & Pain, R. H. Relation between stability, dynamics and enzyme activity in 3-phosphoglycerate kinases from yeast and Thermus thermophilus. *J. Mol. Biol.* **220,** 531–538 (1991).
15. Wrba, A., Schweiger, A., Schultes, V., Jaenicke, R. & Zavodszky, P. Extremely thermostable D-glyceraldehyde-3-phosphate dehydrogenase from the eubacterium Thermotoga maritima. *Biochemistry* **29,** 7584–7592 (1990).
16. Lin, S. & Saunders, W. H. Tunneling in elimination reactions—structural effects on the secondary beta-tritium isotope effects. *J. Am. Chem. Soc.* **116,** 6107–6110 (1994).
17. Saunders, W. H. Calculations of isotope effects in elimination reactions. New experimental criteria for tunneling in slow proton transfers. *J. Am. Chem. Soc.* **107,** 164–169 (1985).
18. Rucker, J. & Klinman, J. P. Computational study of tunneling and coupled motion. *J. Am. Chem. Soc.* **121,** 1997–2006 (1999).
19. Melander, L. & Saunders, W. H. *Reaction Rates of Isotopic Molecules* (Krieger, Malabar, FL, 1987).
20. Vihinen, M. Relationship of protein flexibility to thermostability. *Protein Eng.* **1,** 477–480 (1987).
21. Vol'kenshtein, M. V., Dogonadze, R. R., Madumarov, A. K., Urushadze, Z. D. & Kharkats, Y. I. The theory of enzyme catalysis. *Mol. Biol.* **6,** 347–353 (1972).
22. Hwang, J. K. & Warshel, A. On the relationship between the dispersed polaron and spin-boson models. *Chem. Phys. Lett.* **271,** 223–225 (1997).
23. Antoniou, D. & Schwartz, S. D. Large kinetic isotope effect in enzymatic proton transfer and the role of substrate oscillations. *Proc. Natl Acad. Sci. USA* **94,** 12360–12365 (1997).
24. Borgis, D. & Hynes, J. T. in *The Enzyme Catalysis Process* (eds Cooper, A., Houben, J. & Chien, L.) 293–303 (Plenum, New York, 1989).
25. Bruno, W. J. & Bialek, W. Vibrationally enhanced tunneling as a mechanism for enzymatic hydrogen transfer. *Biophys. J.* **63,** 689–699 (1992).
26. Borgis, D. & Hynes, J. T. Dynamical theory of proton tunneling transfer rates in solution—general formulation. *Chem. Phys.* **170,** 315–346 (1993).
27. Antoniou, D. & Schwartz, S. D. Activated chemistry in the presence of a strongly symmetrically coupled vibration. *J. Chem. Phys.* **108,** 3620–3625 (1998).
28. Somero, G. N. & Siebenaller, J. F. Inefficient lactate dehydrogenases of deep-sea fishes. *Nature* **282,** 100–102 (1979).

Acknowledgements. This work was supported by the NSF (A.K. and J.P.K.) and EC-projects (R.C. and S.B.).

Correspondence and requests for materials should be addressed to J.P.K. (e-mail: klinman@socrates.berkeley.edu).